Available online at www.sciencedirect.com
SCIENCE DIRECT®
Forest Ecology and Management 217 (2005) 129–146
Forest Ecology and Management
www.elsevier.com/locate/foreco

Characterizing and mapping forest fire fuels using ASTER imagery and gradient modeling

Michael J. Falkowski [a,*], Paul E. Gessler [a], Penelope Morgan [a], Andrew T. Hudak [b], Alistair M.S. Smith [a]

[a] *Department of Forest Resources, University of Idaho, 6th and Line St., Moscow, ID 83844-1133, USA*
[b] *Rocky Mountain Research Station, USDA Forest Service, 1221 S. Main St., Moscow, ID 83843, USA*

Received 12 January 2005; received in revised form 30 May 2005; accepted 7 June 2005

Abstract

Land managers need cost-effective methods for mapping and characterizing forest fuels quickly and accurately. The launch of satellite sensors with increased spatial resolution may improve the accuracy and reduce the cost of fuels mapping. The objective of this research is to evaluate the accuracy and utility of imagery from the advanced spaceborne thermal emission and reflection radiometer (ASTER) satellite sensor, and gradient modeling, for mapping fuel layers for fire behavior modeling with FARSITE and FLAMMAP. Empirical models, based upon field data and spectral information from an ASTER image, were employed to test the efficacy of ASTER for mapping and characterizing crown closure and crown bulk density. Surface fuel models (National Forest Fire Laboratory (NFFL) 1–13) were mapped using a classification tree based upon three gradient layers; potential vegetation type, cover type, and structural stage. The final surface fuel model layer had an overall accuracy of 0.632 ($K_{HAT} = 0.536$). Results for the canopy fuel empirical models developed here suggest that vegetation indices incorporating visible wavelengths (i.e. the green red vegetation index (GRVI)) are suitable for predicting crown closure and crown bulk density ($r^2 = 0.76$. and 0.46, respectively).

Keywords: Forest fire; Fuels; Remote sensing; Gradient modeling; ASTER; Fuel model; Crown bulk density; Crown closure

1. Introduction

Wildland fire is an important issue facing local and regional land managers in the United States. Fires occurring in many parts of the western United States today are often more severe than fires that occurred before the advent of effective fire suppression and intensive land use (Arno and Brown, 1989; Hessburg et al., 2000). Increased fire size and severity coupled with an increase in the number of people living in the wildland–urban interface has resulted in millions of dollars of damage to property and loss of life throughout the western United States in recent years. In 2002 and 2003, federal agencies spent an estimated $1.6 and $1.3 billion on fire suppression, respectively

* Corresponding author. Tel.: +1 208 885 4946.
E-mail address: falk4587@uidaho.edu (M.J. Falkowski).

0378-1127/$ – see front matter © 2005 Elsevier B.V. All rights reserved.
doi:10.1016/j.foreco.2005.06.013

(NIFC, 2003). Current estimates suggest that there are more than 15 million hectares of wildlands at risk to catastrophic wildfire (GAO, 1999). As human populations move closer to the edges of wildlands, their lives and property become increasingly threatened by wildfire. To reduce fire risk to people and their homes, land managers must prioritize areas for fire mitigation and hazardous fuels reduction.

In 2000, the US Department of Agriculture, the US Department of Interior and the National Association of State Foresters collaborated to develop the National Fire Plan (www.fireplan.gov). Along with post-fire rehabilitation and maintaining firefighting preparedness, the goals of the National Fire Plan include reducing fuels in at-risk areas, particularly in and around the wildland–urban interface (Bisson et al., 2003). More recently, the Healthy Forests Restoration Act facilitates hazardous fuels reduction and forest and rangeland restoration (Starbuck et al., in press). Each year, initiatives such as the National Fire Plan and Healthy Forests Restoration Act provide funds to local fire districts to increase fire suppression capabilities and implement fuels reduction projects (USDA, 2003). In order to utilize these funds efficiently, land managers need cost-effective methods for mapping and characterizing fire fuels quickly and accurately. Some of the approaches with the best potential for accomplishing this involve the integration of remote sensing (RS), geographic information system's (GIS), and environmental gradient modeling. Such analyses could provide consistent maps of fire fuel conditions across a diversity of land ownerships, and provide a means to update such maps at regular intervals.

2. Previous work

2.1. Fuels mapping

Some of the most important factors influencing fire hazard and fire risk are the type, composition, and distribution of fuels (Chuvieco and Congalton, 1989). Wildland fuels are typically divided into three strata: ground fuels, surface fuels, and crown fuels (Pyne et al., 1996). Ground fuels consist of roots, duff, and buried woody debris. Fires burning in this stratum usually exhibit slow rates of spread. Surface fuels are composed of leaf litter, coarse woody debris, seedlings, saplings, and herbaceous vegetation. Most wildland fires start in, and are carried by, surface fuels. Overstory trees and shrubs comprise the crown fuel strata. Fires burning in the crown fuel strata are often extremely intense and nearly impossible to control (Pyne et al., 1996). Since fuel stratum relationships are extremely complex, fire managers often describe fuels by grouping vegetation communities, based upon similar potential fire behavior, into fuel types (Riano et al., 2002) or fuel models (e.g. National Forest Fire Laboratory (NFFL 1–13) (Anderson, 1982). However, since the distribution and accumulation of fuels is highly variable (Brown and Bevins, 1986) and highly dependent upon vegetation type, stand history, and disturbance regime (Keane et al., 2001; Brandis and Jacobson, 2003), fuel quantity and distribution are not often directly related to vegetation types (Pyne et al., 1996).

2.2. Field mapping of fuels

Fuels can be mapped through extensive field inventory with sampling and statistical inference. Although these techniques are successful, the amount of time and money required render their implementation impractical for many land managers (Miller et al., 2003). The development of remote sensing technologies could potentially reduce the cost and time required to map fuels on the ground (Keane et al., 2001) by providing a continuous dataset from which to assess fuel conditions across entire landscapes. In addition, remote sensing technology has the potential to update fuel maps quickly and consistently in areas where conditions are dynamic due to logging, fire, or other changes and disturbances.

2.3. Remote sensing of crown fuels

Traditionally, interpretation of aerial photography coupled with field data has been the primary method used to map fire-related tree crown variables (Riano et al., 2003) such as crown bulk density, crown closure, and canopy height. More recently empirical methods, which are less labor intensive, have been used to estimate these variables from Landsat thematic mapper (TM) and systeme probatoire d'observation de la terre (SPOT) high resolution visible (HRV) data (Riano et al., 2003). For example, Franklin et al. (2003) mapped various stand attributes, including

canopy height and crown closure, through implementation of empirical relationships between single band Landsat reflectance and canopy characteristics. Miller et al. (2003) successfully mapped structural stage classes in Arizona by running Landsat TM data through a clustering algorithm. Xu et al. (2003) examined the relationship between crown closure and Landsat single band reflectance as well as the relationship between crown and vegetation indices. They concluded that visible wavelengths were better suited for predicting crown closure than near-infrared or mid-infrared wavelengths. This was attributed to the phenological stage of the grass understory (senesced) at the time of image acquisition (late summer).

2.4. Remote sensing of surface fuels

The inability of optical sensors, such as Landsat TM and multi-spectral scanner (MSS), to penetrate the forest canopy (Miller et al., 2003) limits their utility for mapping surface fuels where tree canopies are present (Keane et al., 2000). As a result, most studies using remote sensing to characterize surface fuels first classify an image into vegetation categories, then and assign fuel types or fuel models to each category (Keane et al., 2001). Chuvieco and Salas (1996) characterized fuel types through the classification of Landsat TM data. Chuvieco and Congalton (1989) and Castro and Chuvieco (1998) used similar methods to map fuel types in Spain and Chile, respectively. Wilson et al. (1994) applied maximum likelihood decision rules to a Landsat MSS image to directly classify fuel types across Wood Buffalo National Park, Canada. Riano et al. (2002) improved a fuel type classification by incorporating two seasonal Landsat TM images, to account for phenological differences in vegetation, into a classification algorithm. Remotely sensed hyperspectral data have also been used to map fuel types and vegetation moisture content for a chaparral community in Southern California (Roberts et al., 1998; Roberts et al., 2003).

2.5. Gradient modeling of fuels

Gradient modeling refers to the use of environmental gradients (topographical, biogeochemical, biophysical, and vegetational) to model the occurrence of natural phenomena (Keane et al., 2000) such as vegetation types (Curtis, 1959) or the distribution of soil types (Jenny, 1941; McSweeney et al., 1994). This approach has been used with moderate success in the classification of fuel types and fuel loading (Kessell, 1979; Keane et al., 2001).

Environmental gradients can be broken into three types: indirect gradients, direct gradients, and resource gradients (Austin and Smith, 1989). Indirect gradients, such as elevation, do not directly influence vegetation types or fuel types. However, elevation influences temperature gradients (direct gradient), which have a direct influence on vegetation. Resource gradients refer to gradients such as nutrients and water, which are utilized by vegetation (Austin and Smith, 1989; Keane et al., 2002). Direct and resource gradients are extremely useful when mapping ecological phenomena, but have been under utilized in natural resource disciplines due to complexities associated with their parameterization (Keane et al., 2002). Instead, indirect gradients, such as potential vegetation type (PVT), are used as surrogates for direct and resource gradients.

The PVT of a site is dictated by both direct and resource gradients, which ultimately impact the vegetation type and fuel loading (amount of fuel present in terms of weight per unit area) occurring on a site (Kessell, 1979). High fuel loading, for example, is often found where biomass production exceeds microbial decomposition (characterized by moisture and temperature gradients) and where it has been a long time since the last major fire or other disturbance (Keane et al., 2001). Indirect gradient modeling has been used to model fuel characteristics in Glacier National Park, Montana (Kessell, 1979). However, modeling landscape attributes directly on resource gradients is rarely performed due to difficulties associated with the identification and quantification of these gradient types (Keane et al., 2002).

2.6. Integrated fuels mapping

The integration of remote sensing and gradient modeling may increase the accuracy of fuels mapping projects. For example, Keane et al. (2002) integrated remote sensing and gradient modeling to map fuels across the Gila National Forest in New Mexico. This approach incorporates three indirect gradient layers (the vegetation triplet): potential vegetation type (PVT), cover type (CT), and structural stage (SS). PVT is a site classification based upon the climax

vegetation that would be found on a site in the absence of disturbance (Keane et al., 2000; Smith et al., 2003). CT describes the dominant species found on a site, and SS refers to the current canopy structure of a site (e.g. multiple or single canopy layer). PVT is directly related to the biophysical setting of a site, which ultimately determines site productivity and decomposition rate, and therefore has a large impact on fuel characteristics (Keane et al., 2000). CT is important for fuels mapping because dead woody debris and litter are directly related to the dominant tree species found on the site (Keane et al., 2000). The potential of a surface fire spreading to the crown is highly dependent upon the vertical structure of the stand, which is described here by SS. This triplet approach has been used to assess the hazard of forest disease outbreak and vulnerability to fire in the Columbia basin (Hessburg et al., 2000). It has been used in the Gila National Forest and the Selway-Bitteroot Wilderness to map fuels and input layers required to run FARSITE (Keane et al., 2000; Keane et al., 2001).

2.7. Fuels mapping objective

Remote sensing-based fuels mapping has typically employed one of the Landsat sensors (MSS, TM, or ETM+) to map fuels characteristics (Riano et al., 2003). Although these sensors are effective, and widely applicable to many environmental mapping and monitoring situations, the development and launch of new sensors with improved spatial and spectral resolutions may improve the accuracy (Chuvieco and Congalton, 1989) and reduce the cost (Zhu and Blumberg, 2001) of forest fuels mapping. ASTER, a sensor aboard NASA's Terra platform (see specifications Table 1), has untested potential for characterizing and mapping forest fuels. The visible and near-infrared telescope (VNIR), which collects data with a spatial resolution of 15 m in the green (0.52–0.60 μm), red (0.63–0.69 μm), and near-infrared (0.76–0.86 μm) portions of the electromagnetic spectrum, should be particularly useful for obtaining information about vegetation (Rowan and Mars, 2003), and may prove successful in mapping fuel characteristics.

The objective of this paper is to evaluate the accuracy and utility of ASTER imagery coupled with gradient modeling for mapping fuels layers for fire modeling with FARSITE (Finney, 1998) and FLAMMAP (Finney et al., 2003), which are modeling programs used to spatially simulate and predict fire behavior based upon inputs depicting topography (i.e. elevation, slope, aspect), fuels (surface and crown), and weather (i.e. wind, humidity). This paper describes and evaluates methods used to spatially predict surface fuel models (NFFL 1–13, Anderson, 1982) and crown fuel characteristics (crown bulk density and crown closure) required to run FARSITE and FLAMMAP. We create potential vegetation type, cover type, and structural stage indirect gradient layers, which are implemented as predictor layers within the surface fuel model classification process. Field data from a Moscow Mountain study area in Idaho are then used to evaluate the results of the surface fuels mapping process through a quantitative accuracy assessment. In addition, canopy fuel related variables are predicted across the Moscow Mountain study area through the implementation of empirical relationships between spectral vegetation indices and field measurements quantifying canopy fuels.

Table 1
ASTER specifications (adapted from Abrams, 2003)

Spectral region	Spatial resolution (m)	Channel	Bandwidth (μm)
Visible–near-infrared (VNIR)	15	1	0.52–0.60
	15	2	0.63–0.69
	15	3	0.76–0.86
Short-wave Infrared (SWIR)	30	4	1.60–1.70
	30	5	2.145–2.185
	30	6	2.185–2.225
	30	7	2.235–2.285
	30	8	2.295–2.369
	30	9	2.360–2.430
Thermal infrared (TIR)	90	10	8.125–8.475
	90	11	8.475–8.825
	90	12	8.925–9.275
	90	13	10.25–10.95
	90	14	10.94–11.65

3. Materials and methods

3.1. Study area

Moscow Mountain (Fig. 1), the extreme western extension of the Clearwater Mountains, is located

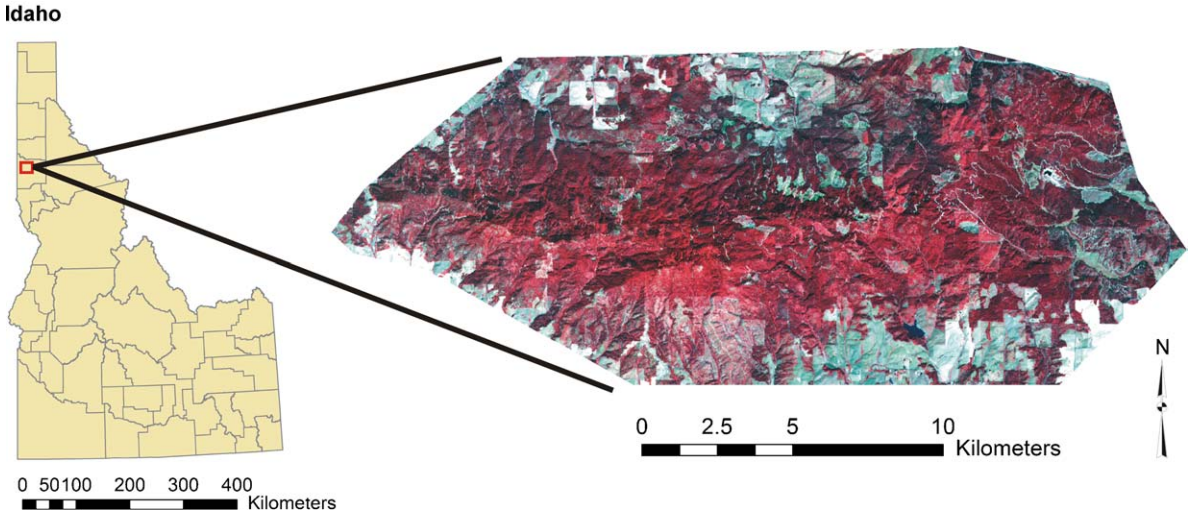

Fig. 1. Moscow Mountain study area—an ASTER image displayed in a 3 (NIR), 2 (red), 1 (green) false color composite.

approximately 9 km northeast of the city of Moscow, Idaho (Latitude 46°44′N, Longitude 116°58′W). This area encompasses approximately 25,000 ha of mixed temperate conifer forest and is topographically diverse, with gentle to moderately steep slopes on many different aspects. There are also many homes, buildings, and private properties interspersed with large tracts of forestland. This area's diverse management history and land ownership has created a complex mosaic of forest structure and fuel, making it an excellent location to test the efficacy of satellite sensor imagery for mapping forest fuels. Some parts of the forest have been logged multiple times; others have had little logging or no logging. Prescribed burning is used often as part of forest management practices on some, but not all lands to accomplish site preparation and other vegetation management goals. For instance, the University of Idaho's Experimental Forest implements prescribed burns across 1–2% of their forest annually. The resulting mixed conifer forests are very diverse in species composition and forest structure, and surface and crown fuel loading vary greatly.

3.2. Sample design

One hundred and sixty-two field plots were located using a two-stage (stratified systematic) sample design. For the first stage, nine strata were constructed based upon unique combinations of three elevation strata and three solar insolation strata. Elevation and solar insolation were chosen because they quantify biophysical gradients (e.g. temperature, moisture, and energy) over the study area. They also characterize the biophysical potential of a site, and therefore have a large impact upon fuel dynamics such as fuel type, fuel loading, and fuel moisture content (Keane et al., 2000). Solar insolation was calculated from a 30 m USGS digital elevation model (DEM) for the growing season (mid-April–late September) using the solar analyst (HEMI, 2000) software package. Solar insolation and elevation were each partitioned into three individual strata (Table 2) using a quantile classifier (33%). The resulting strata were then crossed to provide nine unique combinations of the three solar insolation and three elevation strata for each 30 m grid cell. For the second sampling stage, leaf area index (LAI) values, derived from an empirical model using the normalized difference vegetation index (NDVI) derived from a Landsat enhanced thematic mapper (ETM+) image (Pocewicz et al., 2004), were calculated within each of the nine strata and ranked

Table 2
Strata classification break values

Strata breaks	Elevation (m)	Solar insolation (W/m^2)
Low	<896	<7063
Medium	896–978	7063–7276
High	>978	>7276

from low to high. Pixels were then systematically selected across each stratum's LAI gradient. Sampling in such a manner produced spatially random plot locations across the full range of canopy conditions throughout the study area.

3.3. Data collection

The development of new technologies, and the need for up-to-date fuels information, has lead to the creation of new initiatives aimed at mapping and monitoring fuels and fire effects nationwide. In order to be effective, such initiatives need to collect data in a consistent manner. As a result, the USDA Forest Service developed a new sampling protocol, called fire effects monitoring and inventory protocol (FIREMON) (http://fire.org/firemon/). This new sampling protocol is structured so it is applicable to many fuel and vegetation conditions.

Actual and potential vegetation type, surface fuel model, slope, and aspect were assessed and recorded at each of the 162 field plots. An intensive inventory of surface and crown fuels was conducted at 81 of the 162 field plots with sampling procedures adapted from the FIREMON sampling protocol. A 405 m^2 fixed-radius plot, which has a radius of 11.35 m (Fig. 2), was used for tree measurements. The diameter at breast height (DBH), percent live crown, species, distance from plot center, bearing, and quadrant (NE, SE, SW or NW) was recorded for every tree or snag $\geq$2.7 cm DBH within the fixed-radius plot. A variable radius plot (15 m^2/ha) was used to identify large, influential trees or snags outside the fixed-radius plot. The same variables were recorded for each tree or snag captured in the variable radius plot. Height, height to live crown, and both the major and minor crown diameters were measured for the trees with the largest and smallest DBH for each species within each quadrant. Crown density was measured using a spherical densiometer at the northern, eastern, southern, and western corners of the fixed-radius plot (Fig. 2).

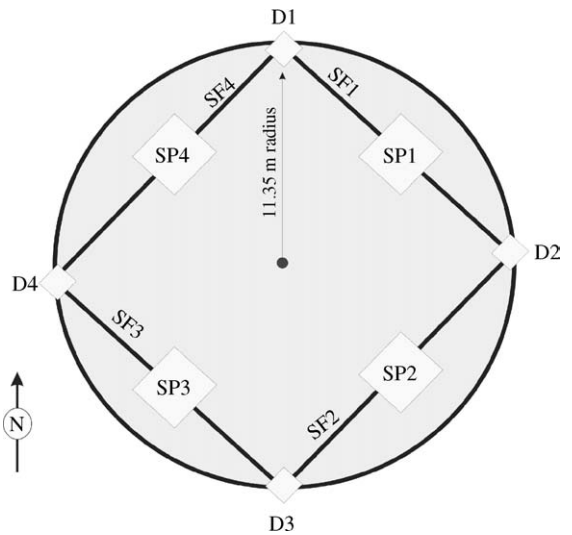

Fig. 2. Plot layout diagram: SF1–4, surface fuel transects; D1–4, densiometer reading locations; SP1–3, vegetation subplot locations.

Downed woody debris (DWD) was measured along four transects (Fig. 2). One-hour fuels (DWD 0–0.64 cm diameter) and 10-h fuels (DWD 0.64–2.54 cm diameter) were tallied along the first 1.8 m of each transect. One hundred-hour fuels (DWD 2.54–7.62 cm diameter) were tallied along the first 4.6 m of each transect. The diameter of 1000-h fuels (DWD > 7.62 cm diameter) was recorded along the entire length of each transect. Litter and duff depths were measured 4.6 m from the beginning of each 16.1 m transect. Visual estimates of percent canopy cover by vegetation class (sapling, seedling, shrub (tall, medium and low), grass, forb, fern, moss/lichen, and litter) were made within four 4 m × 4 m subplots centered over the midpoint of each DWD transect (8 m from beginning).

After collection, the data were divided randomly into two datasets: a classification dataset (66% of the original data or 107 plots), and an accuracy assessment dataset (33% of the original data or 55 plots).

3.4. Data analysis

3.4.1. Preprocessing

A Level 1B (VNIR registered radiance at the sensor) ASTER image, acquired on September 10, 2002, was imported into the ERDAS Imagine (Leica, 2004) image processing software using the built-in ASTER import dialog. Geometric correction was performed and radiance values were converted to top-of-atmosphere reflectance. Since this study only used imagery acquired at a single point in time, and low atmospheric water content and clear skies were present at the time of image acquisition, an atmospheric correction was not performed. Vegetation

indices, such as the normalized difference vegetation index (NDVI [NIR − R/NIR + R]), simple ratio (SR [NIR/R]), and green–red ratio vegetation index (GRVI [green − red/green + red]), were calculated from the processed ASTER image.

A 10-m USGS DEM was resampled to the same resolution as the ASTER image (15 m) using a nearest neighbor algorithm within ArcGIS. The resampling procedure was performed to ensure each input layer (CT, SS, PVT) and output layer (crown closure, crown bulk density, and surface fuel model) had the same spatial resolution.

3.4.2. Surface fuel model layer development

Surface fuel models were mapped across the study area by implementing the aforementioned "vegetation triplet" (PVT, SS, CT) (Keane et al., 2000). A supervised classification (maximum likelihood) routine was used to map CT and SS from the ASTER imagery. The PVT and final surface fuel model layers were developed using a classification tree algorithm within the S-Plus® (Insightful, 2000) statistical software package. The classification tree algorithm uses training sets to develop classification rules by recursively partitioning training data into categories, with each split chosen to maximize differences between the two resultant groups (Lawrence and Wright, 2001), and sub-setting the training data into more homogenous groups. Classification trees are ideal for modeling and mapping landscape attributes such as PVTs and surface fuel models because the data inputs can be either categorical or continuous and are not required to meet traditional statistical assumptions such as normality or homoscedasticity (Keane et al., 2002). Classification trees are also able to deal with nonlinearity and are fairly easy to implement and interpret as compared to other multivariate techniques (McBratney et al., 2003). In addition, the decision rules created through classification trees can be interpreted and linked to environmental process across entire landscapes. A detailed discussion of the techniques used to produce each layer follows.

3.4.2.1. Potential vegetation type layer development. PVT (series level groups of habitat types based upon Cooper et al. (1991) (Table 3) was mapped across our study area through the implementation of classification tree decision rules using topographic variables (elevation, slope, and aspect) and basic soils information (presence or absence of volcanic ash cap) as independent variables at each field plot within the classification dataset. PVT classification rules were derived from a classification tree using slope, aspect, and elevation as predictor variables. Elevation, slope, and aspect were chosen to classify PVT because they are surrogates for biophysical setting, and therefore directly influence the vegetation community composition (Smith et al., 2003) and ultimately surface fuel models. Areas corresponding to water bodies were masked out from the PVT classification. Optimal tree size was determined by examining cost complexity plots produced via the prune function in S-Plus®.

Local forest managers emphasized that the presence of volcanic ash cap soil types, which have higher nutrient levels and water holding capacities (Page-Dumroese et al., 1996), strongly influence the occurrence of the western redcedar (*Thuja plicata)* PVT across the study area. Therefore, US Department of Agriculture Natural Resource Conservation Service (USDA NRCS) digital soils maps (USDA NRCS, 2003) depicting the presence or absence of volcanic ash cap soils were also incorporated into the suite of potential explanatory variables used in the decision tree modeling. The final PVT classification rules (Fig. 3) were then applied across the entire study area to create the final PVT layer (Fig. 4).

Table 3
Classification schemes

Classification	Variable
Potential vegetation type (PVT)	*Pseudotsuga menziesii* (PSME) *Abies grandis* (ABGR) *Thuja plicata* (THPL)
Cover type (CT)	Grass Shrub *Pinus ponderosa/Pseudotsuga menziesii* (PIPO/PSME) *Pseudotsuga menziesii/Abies grandis* (PSME/ABGR) *Abies grandis/Thuja plicata* (ABGR/THPL) Water
Structural stage (SS)	Open stem exclusion (OSE) Stand initiation (SI) Young multi-story (YMS) Old multi-story (OMS) Water

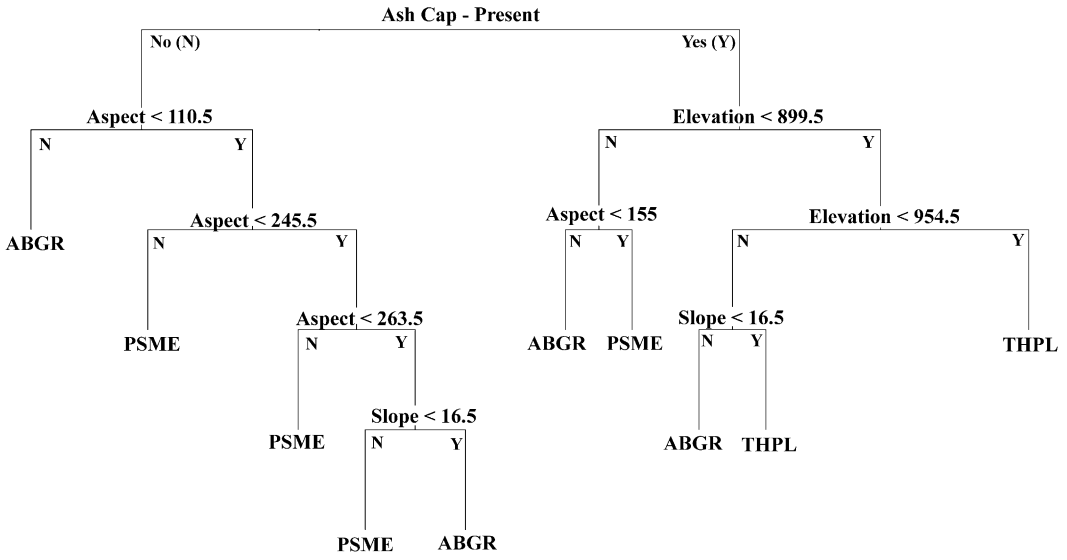

Fig. 3. Potential vegetation type (PVT) classification tree decision rules. Predictor variables used in the classification include ash cap soil (present or absent), elevation (m), slope (%), and aspect (degree).

3.4.2.2. Cover type and structural stage layer development. Cover types, adapted from the Idaho GAP analysis vegetation classification scheme (GAP, 2004) (Table 3), and structural stages, based upon the Interior Columbia Basin Management Project's (ICBMP) structural stage classification scheme (O'Hara et al., 1996) (Table 3), were mapped across the Moscow Mountain study area through the implementation of a maximum likelihood supervised classification algorithm in ERDAS IMAGINE® (Leica, 2004). Field data (107 plots) were used as training data within the maximum likelihood classification algorithm.

The final PVT, CT, and SS layers (Fig. 4) were input as predictor variables to a classification tree algorithm used to derive surface fuel model classification rules based upon the field data. These classification rules (Fig. 5) were then applied across the entire study area to create the final surface fuel model (FM) layer (Fig. 6).

3.4.3. Crown fuel layer development

Empirical models (ordinary least squares regression), based upon field data and ASTER satellite data, were employed to test the efficacy of ASTER satellite data for mapping and characterizing crown closure and crown bulk density. Crown closure and crown bulk density were calculated at the plot level based upon field densiometer measurements (for crown closure) and the forest vegetation simulator (Stage, 1973, for crown bulk density). Single band reflectances (green, red, and near-infrared (NIR)) and vegetation indices (NDVI, GRVI and SR) were tested as predictor variables. Model coefficients were extracted (Table 4) from the best model for each response variable and incorporated into an algorithm to create the final crown closure and crown bulk density layers (Fig. 6).

3.5. Accuracy assessment and model evaluation

The accuracy assessment data set (55 field plots) was used to quantitatively assess the accuracy of each layer (PVT, CT, SS, and surface FM) produced through the surface fuels mapping process. Error matrices quantifying overall accuracy, omission errors, and commission errors were examined to evaluate the accuracy and performance of each classification (Congalton and Green, 1999). In addition, the kappa statistic (K_{HAT}) (Cohen, 1960), which determines if classification results are significantly better than results arrived at by pure chance (i.e. a random result) (Lillesand and Kiefer, 1994; Jensen, 1996; Congalton and Green, 1999), was derived for each classification.

The performance of each empirical model for crown fuel prediction was evaluated based upon the

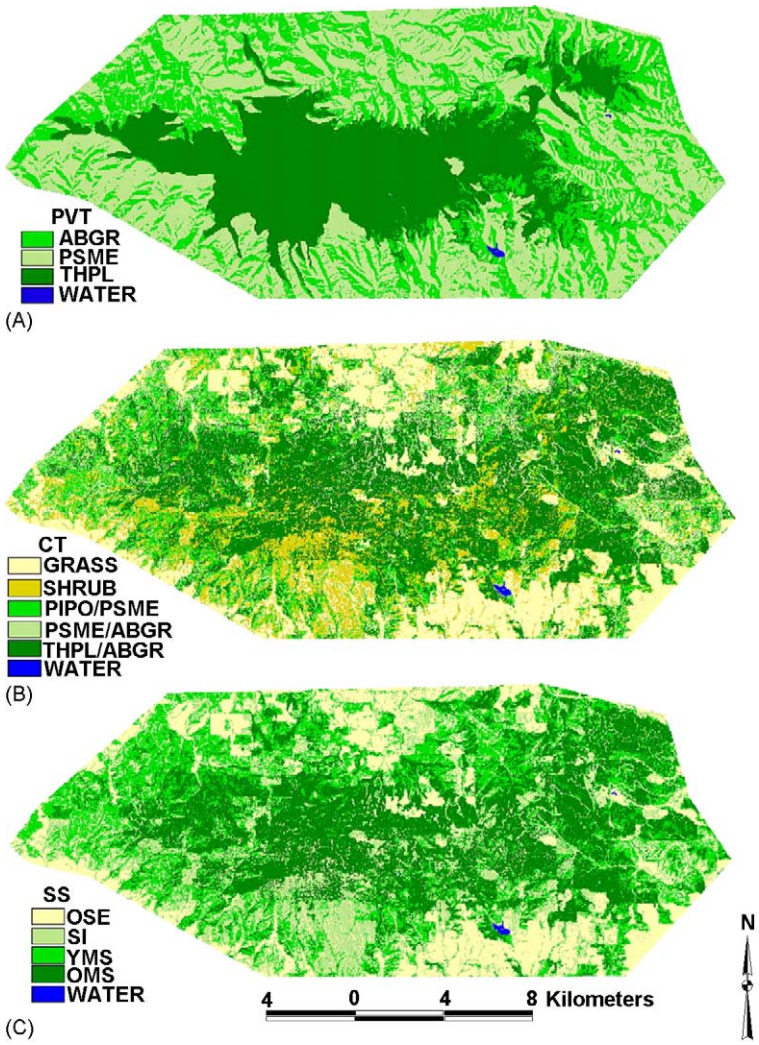

Fig. 4. Moscow Mountain surface fuel model predictor layers. (A) Potential vegetation types (PVT), (B) cover types (CT), (C) structural stages (SS).

coefficient of determination (r^2), root mean square error (RMSE), and the Akaike Information Criterion (AIC, Akaike, 1974) statistics. AIC evaluates model fit by penalizing the residual deviance by the number of parameters contained in the model (Akaike, 1974; Gessler et al., 2000). Single AIC values have no meaning. However, when compared between competing models, lower AIC statistics indicate better fitting models (Breck et al., 2003). The delta AIC (Δ_i) statistic is commonly used to assess the statistical difference between competing models, and is calculated as (Burnham and Anderson, 1998):

$$\Delta\mathrm{AIC}_i = \mathrm{AIC}_i - \min(\mathrm{AIC}),$$

where AIC_i is the value for an individual competing model and min(AIC) is the minimum AIC value among the competing models. In general, $\Delta\mathrm{AIC}_i \leq 2$ 2 for a competing model indicates substantial support for that model, $\Delta\mathrm{AIC}_i$ between 3 and 7 indicates moderate support, and $\Delta\mathrm{AIC}_i > 10$ indicates very little support for the model (Burnham and Anderson, 1998; Breck et al., 2003).

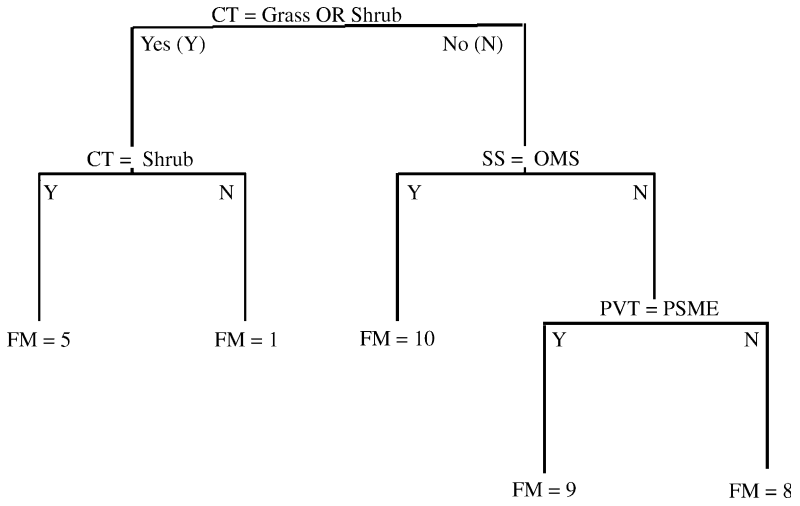

Fig. 5. Surface fuel model (FM) classification tree decision rules. Predictor variables used in the classification include CT, SS, and PVT.

Table 4
Crown fuel regression models with coefficients and model fit statistics

Response variable	Intercept	*b* variable 1	*b* variable 2	r^2	RMSE	AIC	ΔAIC	*p*-value
(1) Crown closure	223.58	−6.02 Green[a]		0.71	18.33%	722.31	15.81	<0.001
(2) Crown closure	144.32	−4.86 Red[a]		0.75	16.87%	708.52	2.02	<0.001
(3) Crown closure	126.82	−1.56 NIR[b]		0.08	32.35%	816.64	110.14	0.006
(4) Crown closure	−96.36	278.65 NDVI[a]		0.69	18.91%	727.50	21.00	<0.001
(5) Crown closure	2.29	375.51 GRVI[a]		0.76	16.68%	706.67	0.17	<0.001
(6) Crown closure	−45.79	27.93 SR[a]		0.65	20.11%	737.70	31.20	<0.001
(7) Crown closure	−22.97	66.61 NDVI[NS]	297.00 GRVI[a]	0.77	16.56%	706.50	–	<0.001
(8) Bulk density	0.2072	−0.0076 Red[a]		0.46	0.0493 kg/m^3	−260.24	2.29	<0.001
(9) Bulk density	0.3339	−0.0103 Green[a]		0.40	0.052 kg/m^3	−251.27	11.26	<0.001
(10) Bulk density	0.1916	−0.0027 NIR[b]		0.06	0.065 kg/m^3	−214.29	48.24	0.02
(11) Bulk density	−0.1642	0.4274 NDVI[a]		0.40	0.0516 kg/m^3	−252.40	10.13	<0.001
(12) Bulk density	−0.0153	0.5926 GRVI[a]		0.47	0.0485 kg/m^3	−262.53	–	<0.001
(13) Bulk density	−0.0957	0.0453 SR[a]		0.43	0.0507 kg/m^3	−255.44	7.09	<0.001
(14) Bulk density	−0.0258	0.0277 NDVI[NS]	0.56 GRVI[a]	0.47	0.049 kg/m^3	−260.58	1.95	<0.001

NS: not significant.
[a] Significant at the 0.001 probability level.
[b] Significant at the 0.01 probability level.

4. Results and discussion

4.1. Classification accuracies

Overall classification accuracies (Table 5) were 0.719 ($K_{HAT} = 0.632$) for CT, 0.684 ($K_{HAT} = 0.589$) for SS, and 0.684 ($K_{HAT} = 0.504$) for PVT. The final surface FM classification had an overall accuracy of

Table 5
Overall accuracy statistics

Layer	Overall accuracy	Kappa
Potential vegetation type (PVT)	0.684	0.504
Structural stage (SS)	0.684	0.589
Cover type (CT)	0.719	0.632
Fuel model (FM)	0.632	0.536

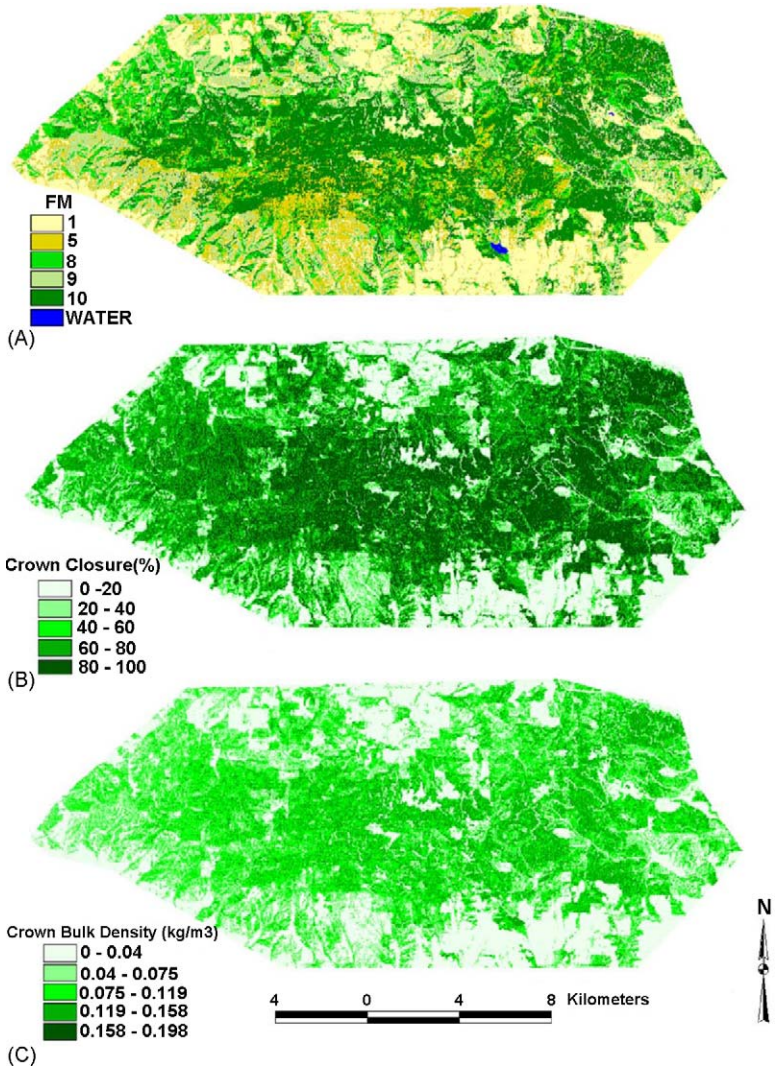

Fig. 6. Moscow Mountain fuel layers. (A) Surface fuel models (FM) (NFFL 1–13), (B) crown closure (%), (C) crown bulk density (kg/m^3).

0.623 (K_{HAT} = .536). Omission and commission errors for categories within each classification (Table 6) were also relatively low.

Classification confusion did occur between the ABGR/PSME and PIPO/PSME categories within the CT classification, which is likely the result of spectral overlap between the ABGR/PSME and PIPO/PSME categories. A relatively large amount of confusion also occurred between the young multi-story (YMS) and old multi-story (OMS) structural stages, as well as between the structural stages. Again, this is the result of the spectral similarity of these categories. Higher accuracies could be obtained by combining spectrally similar cover types (e.g. ABGR/PSME and PIPO/PSME) and structural stages (e.g. YMS and OMS). However, this would likely decrease the overall accuracy of the final surface fuel model classification by decreasing the number of predictor variables the classification tree can use to differentiate fuel models.

In order to determine if the classification tree employed to model PVT produced ecologically meaningful decision rules, the predicted PVT layer

Table 6
Classification error statistics

Class category	Omission error	Commission error
PVT-PSME	0.318	0.2
PVT-ABGR	0.375	0.163
PVT-THPL	0.296	0.1
CT-Grass	0.09	0.087
CT-Shrub	0.333	0.104
CT-THPL/ABGR	0.136	0.057
CT-PIPO/PSME	0.714	0.04
CT-ABGR/PSME	0.8	0.058
CT-Water	0	0
SS-OSE	0.1	0.106
SS-SI	0.5	0.043
SS-YMS	0.579	0.052
SS-OMS	0.067	0.214
SS-Water	0	0
FM-1	0.09	0.086
FM-5	0.333	0.104
FM-8	0.75	0.049
FM-9	0.28	0.021
FM-10	0.214	0.21

was intersected with each classification input (Fig. 7). According to the decision rules, the least moisture tolerant PVT, PSME, occurs on drier aspects (southerly and westerly), moderate slopes (<20%), lower elevations (<1000), and where volcanic ash cap is absent. The THPL PVT (moist sites) occurs in moister sections of the study area (i.e. elevations >900 m where volcanic ash cap is present), while the ABGR PVT (moderately moist sites) typically occurs on northeasterly aspects, with moderate slopes (<20%), in areas of relatively low elevation (<1000 m), and is not dictated by the presence or absence of volcanic ash cap.

The classification tree employed to model surface fuel models also produced logical decision rules (Fig. 8). Surface FM 1 (grass) occurs on the grass CT in the open stem exclusion structural stage, and is typically on the PSME PVT. Surface FM 2 (shrub) is most commonly found on the shrub CT in the stand initiation SS, and is relatively insensitive to changes in PVT. Fuel models 8 (short needle conifer) and 9 (long needle conifer) most commonly occur on the PSME/ABGR and PIPO/PSME cover types in the young multi-story SS. However, FM 8 is typically found on the ABGR and THPL potential vegetation types, while FM 9 occurs on the PSME PVT most often. FM 10 occurs on the THPL/ABGR CT in the old multi-story structural stage, and typically on the ABGR and THPL potential vegetation types.

The CT, SS, PVT, and surface FM layers produced in this study have overall accuracies (Table 5) similar to, or exceeding, studies producing comparable layers. For example, Keane et al. (2002) obtained an overall accuracy of 0.36 ($K_{HAT} = 0.31$) for CT, an overall accuracy of 0.52 ($K_{HAT} = 0.39$) for SS, an overall accuracy of 0.57 ($K_{HAT} = 0.45$) for PVT, and an overall accuracy of 0.55 ($K_{HAT} = 0.45$) for surface FM through the implementation of similar classification methodologies (gradient modeling and Landsat Satellite sensor data, 30-m spatial resolution) across the Gila National Forest, New Mexico. Rollins et al. (2004) predicted surface fuel models by incorporating additional environmental gradients (created through simulation modeling and Landsat satellite data) into a classification tree and achieved an overall accuracy of 0.56 ($K_{HAT} = 0.34$) across the Kootenai River Basin of northwestern Montana. Roberts et al. (2003) attained higher accuracies (overall accuracy of 0.79, $K_{HAT} = 0.72$) by classifying fuel types in southern California using airborne hyperspectral data (AVIRIS).

The differences in accuracies between this study and studies producing similar layers are likely the result of differences in the number of categories within each classification, as well as the relative size of the study areas, and the complexity of vegetation and terrain within each study area. For example, Keane et al. (2002) classified 24 cover types, 12 structural stages, seven potential vegetation types and 10 surface fuel models across the Gila National Forest, an area much larger (>one million hectares) and more complex in both vegetation and topography than the Moscow Mountain study area (25,000 ha, seven cover types).

4.2. Empirical relationships and crown fuel prediction

Green and red reflectances had strong negative correlations with both crown closure and crown bulk density (Table 7), while the NIR reflectance exhibited a weak negative correlation (Pearson's Correlation Coefficient) with both crown closure and crown bulk density. Xu et al. (2003) reported similar correlations between Landsat single band reflectance and crown

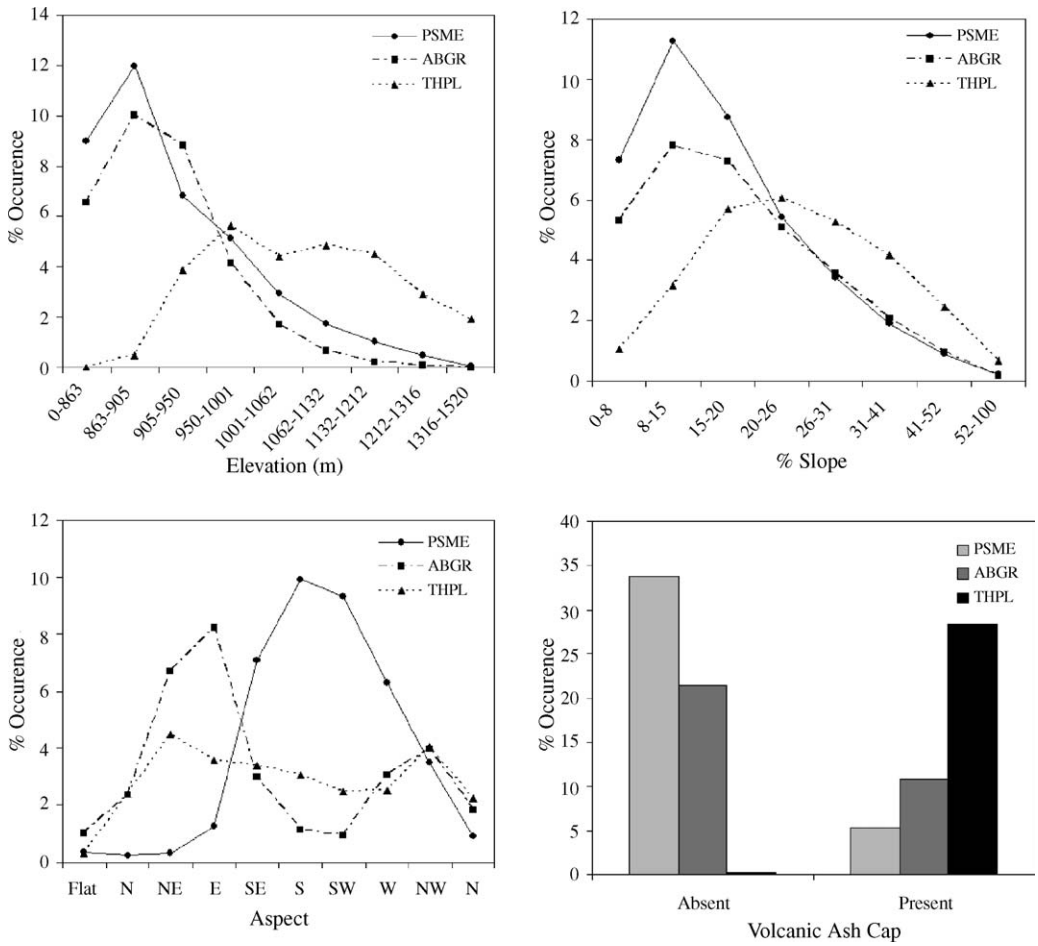

Fig. 7. PVT decision rule results. Graph A—percent occurrence of PVT by aspect, graph B–percent occurrence of PVT by slope (%), graph C—percent occurrence of PVT by elevation (m), graph D—percent occurrence of PVT by volcanic ash cap.

closure. They attributed negative correlations between visible reflectances (green and red) and crown closure to a senesced understory at the time of image acquisition. A senesced understory component is highly reflective across the visible and NIR wavelengths as compared to a photosynthetically active tree canopy. Therefore, as canopy cover decreases, reflectance across the visible and NIR wavelengths increases. Since vegetation index values increase with an increase in photosynthetically active vegetation, positive correlations between these indices and crown fuel variables are expected. Each vegetation index examined in this study did indeed exhibit strong positive correlations with both crown closure and crown bulk density. However, the GRVI index had a stronger correlation with both crown closure and crown bulk density than did the NDVI and SR indices. The weaker correlations between vegetation indices

Table 7
Pearson's correlation coefficients

Variable	Crown closure correlation	Bulk density correlation
Green	−0.842	−0.692
Red	−0.868	−0.687
NIR	−0.297	−0.322
NDVI	0.830	0.635
GRVI	0.871	0.710
SR	0.805	0.647

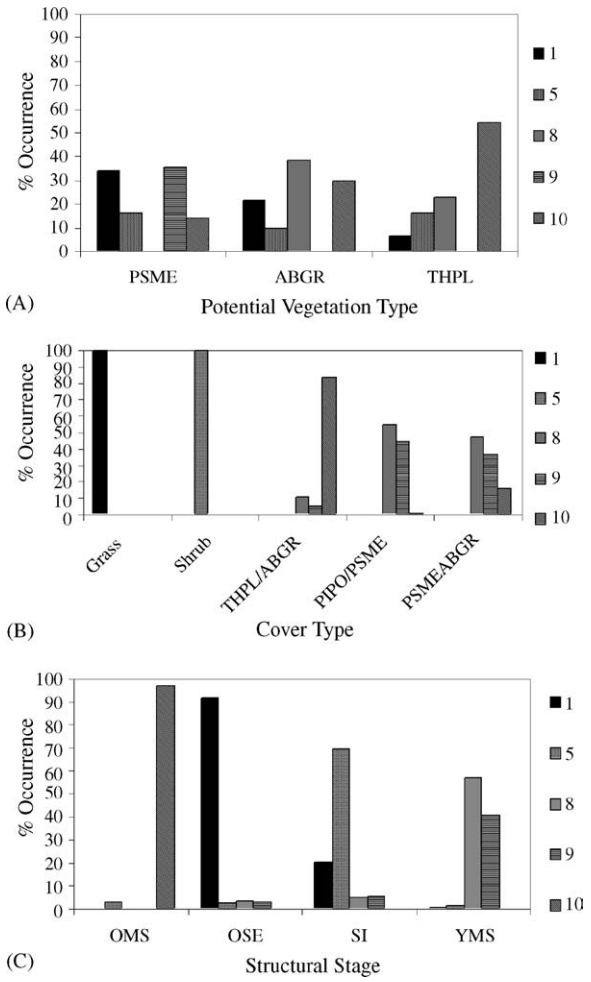

Fig. 8. Surface fuel model (FM) decision rule results. Graph A—percent occurrence of FM by PVT, graph B—percent occurrence of FM by CT, graph C—percent occurrence of FM by SS. 1–10 refer to NFFL fuel model numbers.

incorporating the NIR reflectance (i.e. NDVI and SR) and canopy variables were the result of the weak correlations between NIR reflectance and canopy fuels variables.

In total, seven regression models (Table 4) for each response variable (crown closure and crown bulk density) were compared. Green and red reflectances had a strong relationship to both crown closure and crown bulk density ($r^2 > 0.71$ and $r^2 > 0.46$, respectively). The relationship between NIR reflectance and canopy fuel characteristics was poor (canopy closure $r^2 = 0.08$ and crown bulk density $r^2 = 0.06$). The model containing both the GRVI and NDVI vegetation indices (model 7) as predictors of crown closure obtained the highest r^2, lowest RMSE, and lowest AIC values compared to the other crown closure models (models 1–3). However, since model 5 contained fewer terms and the ΔAIC indicated no substantial difference between model 5 and model 7 (i.e. $\Delta AIC < 2$), model 5 was selected as the optimum model for predicting crown closure. For crown bulk density models 12 and 14 attained similar r^2 statistics. However, since model 12 attained the lowest RMSE, the lowest AIC, and contained fewer terms, it was selected as the optimal model for predicting crown bulk density.

Prior studies have used remote sensing to provide estimates of crown closure. For example, Franklin et al. (2003) demonstrated that significant relationships exist between Landsat band five (MIR) and crown closure for two conifer species (jack pine: $r^2 = 0.30$, $p < 0.005$; white spruce: $r^2 = 0.32$, $p < 0.005$). However, when jack pine was considered alone, a stronger relationship ($r^2 = 0.66$, $p < 0.005$) was achieved with band 4 (NIR) and crown closure. Franklin et al.'s (2003) study was limited in that it only examined relationships between single Landsat bands and crown closure. Xu et al. (2003) investigated correlations between single band Landsat reflectance and several vegetation indices derived from Landsat and found that indices such as NDVI were strongly related to crown closure ($r^2 = 0.69$, $p < 0.05$). The current study demonstrates that the use of vegetation indices that incorporate visible and near-infrared reflectances produce relationships similar in strength to those achieved by Franklin et al. (2003) and Xu et al. (2003). However, use of vegetation indices incorporating visible wavelengths (GRVI) solely or in combination with vegetation indices incorporating near-infrared wavelengths (NDVI) achieve the strongest relationships ($r^2 > 0.76$, $p < 0.005$). As suggested by Xu et al. (2003), this is likely due to the senesced state of the grass understory during the time of image acquisition. Relationships between crown fuel variables and remotely sensed imagery acquired at different times of the year may be quite different than the relationships presented herein.

Only a few previous studies have implemented passive remote sensing or gradient modeling to

estimate crown bulk density. Keane et al. (2002) estimated crown bulk density using the "vegetation triplet" methodology and achieved only a poor relationship ($r^2 = 0.35$, $p < 0.005$). A comparison of this result with the GRVI empirical model (model 6) demonstrates that a significant improvement ($r^2 = 0.47$, $p < 0.005$) is achieved by directly estimating crown bulk density from this vegetation index. More recently, active remote sensing platforms such as light detection and ranging (lidar) have been used to predict crown bulk density, and in general have achieved stronger relationships. For example, Riano et al. (2004) used lidar to estimate crown bulk density in a scots pine (*Pinus sylvestris*) forest and achieved a strong relationship ($r^2 = 0.80$, $p < 0.001$).

5. Conclusions

Overall, ASTER satellite imagery coupled with indirect gradient modeling proved to be an effective tool for mapping and characterizing wildland fire fuels across the Moscow Mountain study area. The methodology presented herein identified surface fuel models and surface fuel model predictor layers (PVT, CT and SS) with accuracies similar to, or slightly higher than, those found in the literature.

Employing empirical relationships between ASTER satellite imagery and field data also proved successful for mapping crown fuels. The crown fuel mapping analysis within the current study demonstrates that significant improvement is achieved through the use of vegetation indices over single bands. In addition, predicting crown closure from vegetation indices relying solely on visible wavelengths results in significant improvements the vegetation indices incorporating NIR reflectance. ASTER's 15-m spatial resolution may indeed be ideal for characterizing crown fuel variables. The characterization of crown fuel variables from finer spatial resolution data (e.g. Ikonos at 4 m) may be problematic due to increases in spectral and spatial variations associated with sub-canopy shadows (i.e. single trees represented by multiple pixels; Asner and Warner, 2003). Conversely, sensors with coarser resolutions (e.g. Landsat at 30 m) may not identify discrete tree and non-tree components (i.e. multiple trees and surface components present within a single pixel) at a level sufficient for characterizing canopy fuel conditions. Additionally, the incorporation of ASTER's 30 m SWIR bands may provide additional discrimination between non-photosynthetic vegetation from background soils. However, we only purchased the VNIR bands, therefore SWIR or TIR data was not evaluated.

When planning canopy fuels mapping projects, managers need to take numerous factors into consideration. If ASTER imagery acquired when the forest understory is senesced is available, managers may obtain excellent results using the techniques presented herein, especially when characterizing canopy fuels with the GRVI index. Due to the limited availability of ASTER imagery, and uncertainties associated with the life span of the ASTER sensor, land managers may need to obtain data acquired by other sensors, such as SPOT or Landsat. However, differences between the spatial and spectral resolutions of these sensors and the spatial and spectral resolutions of the ASTER sensor may compromise the overall precision and accuracy of the final fuels layers. As a result, managers must carefully investigate correlations and relationships between canopy fuel variables and spectral information acquired by the sensor used (ASTER, SPOT, or Landsat).

Slightly higher accuracies have been achieved when classifying fuel types from hyperspectral data (Roberts et al., 2003). Additionally, studies using lidar to estimate crown attributes such as crown bulk density have demonstrated stronger relationships than the relationships presented herein (Riano et al., 2004). Higher accuracies using hyperspectral or lidar data are to be expected given their higher information content. Future fuels mapping efforts may be more successful by integrating multispectral satellite data with hyperspectral data, lidar data, or both. However, the availability of low-cost satellite hyperspectral and lidar datasets is currently limited, and the costs of acquiring and analyzing such data from commercial airborne platforms is impractical for most fuels managers.

Direct and resource gradients could provide better fuel maps than indirect gradients. However, complexities associated with the mathematical and statistical procedures (ordination, principal components analysis, canonical correspondence analysis) required to identify and classify these gradients make their use impractical for many management applications (Keane et al., 2002). As a result, managers may prefer to use easily

quantifiable indirect gradients, such as PVT, when mapping surface fuels. Since the number of classes within each gradient directly impacts its accuracy, and ultimately the accuracy of the final surface fuel classification, careful consideration must also be given to how complex (number of classes) gradients should be; only classes that have the greatest impact on surface fuels should be chosen.

Recent federal initiatives provide funding to state and local governments that develop plans for identifying and mitigating hazards associated with wildland fire in the urban interface. However, this funding is only available to communities that develop spatially explicit assessments of wildfire risk and hazard. The surface and crown fuel data produced by this research can be input into fire behavior simulation programs such as FARSITE (Finney, 1998) and FLAMMAP (Finney et al., 2003) to assess fire hazard, and ultimately fire risk, across the Moscow Mountain study area. Once detailed field data are collected, the methodology presented herein can be applied to any study area with relative ease, making it useful for land managers attempting to carry out fire hazard or fire risk assessments.

Acknowledgements

This research was supported in part by funds provided by the Rocky Mountain Research Station, Forest Service, US Department of Agriculture. The authors also acknowledge partial funding for this work from the following additional sources: the NASA Synergy program, the USDA Forest Service Rocky Mountain Research Station Missoula Fire Sciences Laboratory (RJVA-11222048-140), and a grant (NS-7327) from NASA's Earth Science Applications Division as part of the Food and Fiber Applications of Remote Sensing (FFARS) program managed by the John C. Stennis Space Center.

References

Akaike, H., 1974. A new look at statistical model identification. IEEE Trans. Automat. Control AU-19, 716–722.

Abrams, M., 2003. The advanced spaceborne thermal emission and reflection radiometer (ASTER): data products for the high spatial resolution imager on NASA's Terra platform. Int. J. Rem. Sens. 21, 847–859.

Anderson, H.E., 1982. Aids to determining fuel models for estimating fire behavior. US Department of Agriculture Forest Service, Intermountain Research Station, Ogden, UT. General Technical Report, INT-122, pp. 1–22.

Arno, S.F., Brown, J.K., 1989. Managing fire in our forests-time for a new initiative. J For. 87, 200–207.

Asner, G.P., Warner, A.S., 2003. Canopy shadow in IKONOS satellite observations of tropical forests and savannas. Rem. Sens. Environ. 87, 521–533.

Austin, M.P., Smith, T.M., 1989. A theory of spatial and temporal dynamics in plant communities. Vegetatio 83, 49–69.

Bisson, P.A., Rieman, R.E., Luce, C., Hessburg, P.F., Lee, D.C., Kershner, J.L., Reeves, G.H., Gresswell, R.E., 2003. Fire and aquatic ecosystems of the western USA: current knowledge and key questions. For. Ecol. Manag. 178, 213–229.

Brandis, K., Jacobson, C., 2003. Estimation of vegetative fuel loads using Landsat TM imagery in New South Wales. Aust. Int. J. Wildland Fire 12, 185–194.

Breck, S.W., Wilson, K.R., Andersen, D.C., 2003. Beaver herbivory and its effect on cottonwood trees: influence of flooding along matched regulated and unregulated rivers. River Res. Appl. 19, 43–58.

Brown, J.K., Bevins, C.D., 1986. Surface fuel loadings and predicted fire behavior for vegetation types in the northern Rocky Mountains. US Department of Agriculture, Forest Service, Intermountain Forest and Range Experiment Station, Ogden, UT. Res. Note, INT-358, 9 pp.

Burnham, K.P., Anderson, D.R., 1998. Model Selection and Inference: A Practical Information—Theoretic Approach. Springer-Verlag, New York.

Castro, R., Chuvieco, E., 1998. Modeling forest fire danger from geographic information systems. Geocarto Int. 13, 15–23.

Chuvieco, E., Congalton, R.G., 1989. Application of remote sensing and geographic information systems to forest fire hazard mapping. Rem. Sens. Environ. 29, 147–159.

Chuvieco, E., Salas, J., 1996. Mapping the spatial distribution of forest fire danger using GIS. Int. J. Geogr. Inf. Syst. 10, 333–345.

Cohen, J., 1960. A coefficient of agreement for nominal scales. Educ. Physchol. Meas. 20, 37–40.

Congalton, R.G., Green, K., 1999. Assessing the Accuracy of Remotely Sensed Data. Lewis Publishers, New York, pp. 1–137.

Cooper, S.V., Neiman, K.E., Roberts, D.W., 1991. Forest habitat types on Northern Idaho: a second approximation. US Department of Agriculture–Forest Service, Intermountain Research Station, Ogden, UT. General Technical Report, INT-236, pp. 1–143.

Curtis, J.T., 1959. The Vegetation of Wisconsin: An Ordination of Plant Communities. University of Wisconsin Press, Madision, Wisconsin.

Finney, M.A., 1998. FARSITE: fire area simulator—model development and evaluation. USDA Forest Service, Rocky Mountain Research Station, Fort Collins, CO. Research Paper, RMRS-RP-4.

Finney, M.A., Britten S., Seli, R., 2003. FlamMap2 Beta Version 3.0.1 Fire Sciences Lab and Systems for Environmental Management, Missoula, Montana.

Franklin, S.E., Hall, R.J., Smith, L., Gerylo, G.R., 2003. Discrimination of conifer height, age and crown closure classes using Landsat-5 TM imagery in the Canadian Northwest. Int. J. Rem. Sens. 24, 1823–1834.

GAP, 2004. Idaho GAP analysis project. ID-GAP landcover classification scheme. Available online: <http://www.wildlife.uidaho.edu/idgap/idgap_lccode.asp>.

Gessler, P.E., Chadwick, O.A., Chamran, F., Althouse, L., Holmes, K., 2000. Modeling soil-landscape and ecosystem properties using terrain attributes. Soil Sci. Soc. Am. J. 64, 2046–2056.

Government Accounting Office (GAO), 1999. Western national forests: a cohesive strategy is needed to address catastrophic wildfire threats. GAO/RCED-99-65, Washington, DC. Available online: <http://www.gao.gov> [10-04-2004].

Helios Environmental Modeling Institute (HEMI) LLC (2000). The Solar Analyst 1.0, User Manual.

Hessburg, P.F., Smith, B.G., Salter, R.B., Ottmar, R.D., Alvarado, E., 2000. Recent changes (1930s–1990s) in spatial patterns in interior northwest forests. USA For. Ecol. Manag. 136, 53–83.

Insightful, 2000. S–PLUS 6.0. Professional, Insightful Corporation, Washington.

Jenny, H., 1941. Factors of Soil Formation: A System of Quantitative Pedology. McGraw-Hill, New York.

Jensen, J.R., 1996. Introductory Digital Image Processing: A Remote Sensing Perspective, second ed. Prentice-Hall, New Jersey, pp. 1–318

Keane, R.E., Mincemoyer, S.S., Schmidt, K.M., Long, D.G., Garner, J.L., 2000. Mapping vegetation and fuels for fire management on the Gila National Forest Complex, New Mexico. US Department of Agriculture, Forest Service, Rocky Mountain Research Station, Ogden, UT. General Technical Report, RMRS-GTR-46-CD, pp. 1–126.

Keane, R.E., Burgan, R., van Wagtendok, J., 2001. Mapping wildland fuels for fire management across multiple scales: integrating remote sensing, GIS, and biophysical modeling. Int. J. Wildland Fire 10, 301–319.

Keane, Robert E., Rollins, Matthew G., McNicoll, Cecilia H., Parsons, Russell A., 2002. Integrating ecosystem sampling, gradient modeling, remote sensing, and ecosystem simulation to create spatially explicit landscape inventories. US Department of Agriculture, Forest Service, Rocky Mountain Research Station, Fort Collins, CO. RMRS-GTR-92, 61 pp.

Kessell, S.R., 1979. Gradient Modeling: Resource and Fire Management. Springer Verlag, New York, 1–432.

Lawrence, R.L., Wright, A., 2001. Rule-based classification systems using classification and regression tree (CART) analysis. Photogramm Eng. Rem. Sens. 67, 1137–1142.

Leica, 2004. ERDAS Imagine 8.7. Leica Geosystems AG, St. Gallen, Switzerland.

Lillesand, T.M., Kiefer, R.W., 1994. Remote Sensing and Image Interpretation. John Wiley and Sons, New York, pp. 1–750.

McBratney, A.B., Mendonc Santos, M.L., Minasny, B., 2003. On digital soil mapping. Geoderma 117, 3–52.

McSweeney, K., Gessler P.E., Slater B., Hammer D., Bell J., Petersen G.W., 1994. Towards a new framework for modeling the soil–landscape continuum. In: Factors of Soil Formation: A Fiftieth Anniversary Retrospective. SSSA Special Pub. 33, Chapter 8, pp. 127–145.

Miller, J.D., Danzer, S.R., Watts, J.M., Stone, S., Yool, S.R., 2003. Cluster analysis of structural stage classes to map wildland fuels in a Madrean ecosystem. J. Envrion. Manage. 68, 239–252.

National Inter-agency Fire Center (NIFC). Wildland Fire Season 2002. At a Glance. Available online: <http://www.nifc.gov> [10-04-2004].

O'Hara, L.O., Latham, P.A., Hessburg, P., Smith, B.G., 1996. A structural classification for inland northwest forest vegetation. West. J. Appl. For. 11, 97–102.

Page-Dumroese, D., Jurgensen, M., Harvey, A., 1996. Relationships among woody residues, soil organic matter, and ectomycorrhizae in the cedar–hemlock ecosystem. US Department of Agriculture, Forest Service, Pacific Northwest Research Station. Research Paper, May 1996. PNW-RP-494.

Pocewicz, A., Gessler, P.E., Robinson, A.P., 2004. The relationship between leaf area index and Landsat spectral response across elevation, solar insolation, and spatial scales, in a northern Idaho forest. Can. J. For. Res. 34, 65–480.

Pyne, S.J., Andrews, P.L., Laven, R.D., 1996. Introduction to Wildland Fire. John Wiley & Sons Inc., New York, pp. 1–769.

Riano, D., Chuvieco, E., Salas, J., Palacios-Orueta, A., Bastarrika, A., 2002. Generation of fuel type maps from Landsat TM images and ancillary data in Mediterranean ecosystems. Can. J. For. Res. 32, 1301–1315.

Riano, D., Meier, E., Allgower, B., Chuvieco, E., Ustin, S.L., 2003. Modeling airborne laser scanning data for the spatial generation of critical forest parameters in fire behavior modeling. Rem. Sens. Environ. 86, 177–186.

Riano, D., Chuvieco, E., Condes, S., Gonzalex-Matesanz, J., Ustin, S., 2004. Generation of crown bulk density for *Pinus sylvestris* L. from lidar. Rem. Sens. Environ. 92, 345–352.

Roberts, D., Gardner, M., Regelbrugge, J., Pedreros, D., Ustin, S., 1998. Mapping the distribution of wildfire fuels using AVIRIS in the Santa Monica Mountains Available online:In: http://www.cstars.ucdavis.edu/papers/html/robertsetal1998c/index.html.

Roberts, D.A., Dennison, P.E., Gardner, M.E., Hetzel, Y., Ustin, S., Lee, C.T., 2003. Evaluation of the potential of Hyperion for fire danger assessment by comparison to the airborne visible/infrared imagining spectroradiometer. IEEE Trans. Geosci. Rem. 41, 1297–1310.

Rollins, M.G., Keane, R.E., Parsons, R.A., 2004. Mapping fuels and fire regimes using remote sensing, ecosystem simulation, and gradient modeling. Ecol. Appl. 14, 75–95.

Rowan, L.C., Mars, J.C., 2003. Lithologic mapping in the Mountain Pass, California area using advanced spaceborne thermal emission and reflection radiometer (ASTER) data. Rem. Sens. Environ. 84, 350–366.

Smith, A.J., Gessler, P., Basford, D., 2003. ASPRS 2003 Conference Proceedings. New vegetation mapping tools for the Salmon Challis National Forest.

Stage, A.R., 1973. Prognosis model for stand development. US Department of Agriculture, Forest Service, Intermountain Forest and Range Experiment Station, Ogden, UT. INT-137, pp. 1–32.

Starbuck, M.C., Berrens, R.P., McKee, M., in press. Simulating changes in forest recreation and demand associated economic impacts due to fuels management activities. For. Policy Econ.

US Department of Agriculture (USDA), 2003. National fire plan: managing the impact of wildfires on the communities and environment. Available online: http://www.fireplan.gov.

US Department of Agriculture Natural Resource Conservation Service (USDA NRCS), 2003. Soil Survey Geographic (SSURGO) database for Latah County Area, ID. Fort Worth, TX.

Wilson, B.A., OW, C.F.Y., Heathcott, M., Milne, D., McCaffrey, T.M., Ghitter, G., Franklin, S.E., 1994. Landsat MSS classification of fire fuel types in Wood Buffalo National Park, Northern Canada. Global Ecol. Biogeogr. 4, 33–39.

Xu, B., Peng, G., Pu, R., 2003. Crown closure estimation of oak savannah in a dry season with Landsat TM imagery: a comparison of various indices through correlation analysis. Int. J. Rem. Sens. 24, 1811–1822.

Zhu, G., Blumberg, D.G., 2001. Classification using ASTER data and SVM algorithms; the case study of Beer Sheva, Israel. Rem. Sens. Environ. 80, 233–240.